Gynecologic Oncology Reports 53 (2024) 101391

Contents lists available at ScienceDirect

Gynecologic Oncology Reports

journal homepage: www.elsevier.com/locate/gynor

Molecular profiling of primary endometrioid endometrial cancer and matched lung metastases: *CTNNB1* mutation as a potential driver

Sushmita Gordhandas [a,1], Arnaud Da Cruz Paula [b,1], Elizabeth C. Kertowidjojo [c,d], Fresia Pareja [c], Kimberly Dessources [a,e], Edaise M. da Silva [c], Fatemeh Derakhshan [c,f], Jennifer J. Mueller [a], Nadeem R. Abu-Rustum [a], M. Herman Chui [c], Britta Weigelt [c,*]

[a] *Gynecology Service, Department of Surgery, Memorial Sloan Kettering Cancer Center, New York, NY, USA*
[b] *i3S Instituto de Investigação e Inovação em Saúde, Porto 4200-135, Portugal*[2]
[c] *Department of Pathology and Laboratory Medicine, Memorial Sloan Kettering Cancer Center, New York, NY, USA*
[d] *Department of Pathology, The University of Chicago, Chicago, IL, USA*[2]
[e] *Department of Obstetrics and Gynecology, UNC Health, Chapel Hill, NC, USA*[2]
[f] *Department of Pathology and Cell Biology, Columbia University, New York, NY, USA*[2]

ARTICLE INFO

Keywords:
Endometrial cancer
Lung metastasis
Mutational signatures
CTNNB1
Whole-exome sequencing

1. Introduction

Endometrial cancer (EC) has overtaken ovarian cancer as the leading cause of death from gynecologic malignancy in 2024 in the United States (Siegel et al., 2024). Most ECs are low-grade and early-stage and are considered curable (Siegel et al., 2024; Lu and Broaddus, 2020). Disease stage, grade, histology and, more recently, molecular subtype are the primary clinico-pathologic determinants of prognosis in EC, and distant metastasis is often cited as the worst prognostic factor (Lu and Broaddus, 2020). In a single-institution retrospective review of recurrent EC, the most frequently observed sites of relapse were lymph nodes (46 %), vagina (42 %), peritoneum (28 %) and lung (24 %) (Sohaib et al., 2007). Surveillance, Epidemiology and End Result (SEER) population-based studies of patients with EC reported the most common sites of distant metastases were lung (1.5–1.8 %), followed by liver (0.8–0.9 %), bone (0.6–0.7 %), and brain (0.2 %) (Li et al., 2019; Mao et al., 2020). The molecular processes underpinning distant metastasis in EC are not well understood. Previous phylogenetic analyses by our group and others indicated that metastases typically arose from a common ancestral subclone that was not detected in the matched primary tumor, and acquire additional genetic instability events through defects in DNA repair mechanisms (e.g., microsatellite instability (MSI)), or additional mutagenesis processes (e.g., apolipoprotein B mRNA-editing enzyme catalytic polypeptide, APOBEC) (Gibson et al., 2016; Dessources et al., 2020; Ashley et al., 2019). With increased focus on the molecular classification in EC, a better understanding of the molecular process of lung metastasis may provide an opportunity for targeted therapy and the identification of markers of distant metastasis. In this case report, we sought to characterize the genetic underpinning of two primary ECs compared to their matched lung metastases.

2. Material and methods

Following institutional review board (IRB) approval and written informed consents, a retrospective institutional database from 8/2017–8/2020 was queried for ECs with lung metastasis (n = 100). Pathology reports were reviewed to determine if tissue samples of both the primary EC and matched lung metastases were available for analysis

* Corresponding author at: Department of Pathology and Laboratory Medicine, Memorial Sloan Kettering Cancer Center, New York, NY, USA.
E-mail address: weigeltb@mskcc.org (B. Weigelt).
[1] Equal contribution.
[2] Current address.

https://doi.org/10.1016/j.gore.2024.101391
Received 6 February 2024; Received in revised form 7 April 2024; Accepted 8 April 2024
Available online 10 April 2024

within our institution (n = 7). Hematoxylin and eosin (H&E)-stained sections underwent pathology re-review (E.K., F.D., M.H.C.). For two cases, there was sufficient tissue available for DNA extraction and sequencing. The primary EC, distant metastases (case 1: lung; case 2: lung and brain) and matched normal tissue from these two cases were subjected to microdissection, DNA extraction and whole-exome sequencing (WES; median coverage, 183x; range, 104-216x tumors; 65x and 133x normal tissues) (Table 1). Sequencing data were analyzed for the identification of non-synonymous somatic mutations, copy number alterations, and clonality/ cancer cell fractions of the mutations identified using state-of-the-art bioinformatics tools (Dessources et al., 2020; Safdar et al., 2022). Mutational signatures were identified to assess the underlying mutational processes, based on all somatic mutations (synonymous and non-synonymous) using deconstructSigs, and microsatellite instability (MSI) was defined using MSIsensor, as previously described (Dessources et al., 2020; Ashley et al., 2019). β-catenin immunohistochemical analysis was performed on representative tissue sections of primary EC, and lung/brain metastases, as previously described (Dessources et al., 2020). Immunohistochemistry of the mismatch repair proteins (MMR; i.e., MLH1, PMS2, MSH2, and MSH6) was performed for both cases as well as *MLH1* promoter methylation assessment in the primary EC and metastases of case 2, as described (Dessources et al., 2020).

3. Results

3.1. Case 1

This is a 74-year-old woman diagnosed with stage IA grade 2 endometrioid EC (FIGO 2009). The patient underwent staging surgery followed by intravaginal radiation therapy. Thirty-eight months after her initial surgery, she developed oligometastatic disease at the lung right upper lobe which was resected (Table 1). Morphologically, the primary uterine tumor was composed of low-grade endometrioid glands with prominent morular metaplasia and mature squamous differentiation with keratinization (Fig. 1**A**). In the lung, more areas of solid growth, which focally showed a basaloid appearance, were present, suggestive of transition to higher grade, though these areas were quantitatively insufficient for classification as FIGO grade 3. As the primary EC was *POLE* wild-type, microsatellite stable and p53/*TP53* wild-type, the molecular subtype class was copy number-low/ no specific molecular subtype (NSMP) (Table 1).

WES analysis of the primary FIGO grade 2 endometrioid EC (C1-P) revealed the presence of 81 non-synonymous somatic mutations, including a clonal *PTEN* loss-of-function mutation (p.I303Ffs*4) associated with loss of heterozygosity of the wild-type allele, a clonal *PIK3R1* frameshift insertion mutation (p.E537*), and a subclonal *CTNNB1* mutation (p.G34V; Fig. 1**B**). Consistent with the molecular profiles described for ECs of copy number-low subtype/ NSMP (Cancer Genome Atlas Research Network et al., 2013), the primary tumor harbored few copy number alterations, including copy number gains of chromosome 7 and 10, and a focal amplification of *DIAPH1,* which promotes F-actin polymerization, microtubule stabilization and cell migration, and was also present in the lung metastasis (Fig. 1**C**). In the progression of the primary tumor to the lung metastasis (C1-LM), additional genomic alterations were acquired. The metastasis harbored 75 nonsynonymous somatic mutations, 20 of which were private, including a loss-of-function subclonal mutation in the *FLG* gene which was not present in the primary tumor (Fig. 1**B**). In addition, the subclonal *CTNNB1* gain-of-function hotspot mutation (p.G34V) became clonal in the lung metastasis (Fig. 1**A-B**).

The *CTNNB1* gene encodes the protein β-catenin, which plays a role in cell–cell adhesions. Upon *CTNNB1* hotspot mutations, β-catenin, which is normally expressed at the epithelial cell membrane, is associated with translocation to the cytoplasm and nucleus where it activates downstream transcriptional programs (Costigan et al., 2020). In the primary tumor, immunohistochemistry for β-catenin revealed membranous expression in areas with glandular differentiation with cytoplasmic and nuclear accumulation in morular/squamous areas. Comparatively higher levels of expression in nuclei and cytoplasm were observed in solid/basaloid foci in the lung metastasis, consistent with the increased proportion of tumor cells harboring the *CTNNB1* mutation in the metastases relative to the primary tumor (Fig. 1**A**). Mutational signature analysis of the mutations shared between the primary tumor and lung metastasis revealed a dominant mutational signature 1, which is related to aging/ spontaneous deamination of 5-methylcytosine (Alexandrov et al., 2013). In addition to the dominant aging signature, the mutations unique to the primary tumor harbored a secondary mutational signature 6 and a tertiary signature 15, both associated with microsatellite instability (Fig. 1**D**).

3.2. Case 2

This is a 62-year-old woman with stage IVB grade 3 endometrioid EC (FIGO 2009) metastatic to the lung at diagnosis. Six months after surgery and chemotherapy, the patient developed paratracheal lymphadenopathy. She received immunotherapy and was diagnosed with an isolated brain metastasis nine months after initial diagnosis, which was treated with resection followed by radiation therapy (Table 1). Histopathologic review revealed the primary uterine tumor to be composed of a glandular component with typical low-grade endometrioid morphology, juxtaposed with a high-grade component composed of basaloid tumor cells with a nested and solid cohesive growth pattern and extensive tumor cell necrosis. Tumor nuclei were relatively monotonous and round, with prominent nucleoli, and abundant mitotic figures were present. Despite the spatially distinct low-grade and high-grade components, the tumor cells did not show discohesive growth characteristics of de-differentiated EC; hence, the diagnosis was rendered as FIGO grade 3 endometrioid EC. Metastases in lung and brain were comprised of only the high-grade solid component. The morphologic features (i.e. solid/ nested growth of basaloid cells and conspicuous tumor necrosis) were reminiscent of the recently described FIGO grade 3 endometrioid ECs resembling pilomatrix carcinoma, which have been associated with aberrant β-catenin expression and *CTNNB1* driver mutations (Weisman et al., 2022).

All three tumor samples lacked PMS2 and MLH1 expression by immunohistochemistry (Fig. 2**A**), were MSI-high based on WES (MSIsensor scores $\geq$ 3.5; Fig. 2**B**), had stable genomes (Fig. 2**C**), and were of

Table 1
Clinicopathologic features of the endometrial cancers with lung metastases included in this study.

Case ID	Age at diagnosis (years)	Histology	Myometrial invasion	LVSI	FIGO 2009 Stage	MMR IHC	p53 IHC	Timing lung metastasis	Molecular subtype
1	74	FIGO grade 2 endometrioid	6/14 (43 %)	Yes	IA	Retained	WT	Recurrence	CN-L/ NSMP
2	62	FIGO grade 3 endometrioid	26/26 (100 %)	Yes	IVB	MLH1/PMS2 loss	WT	At diagnosis	MSI-H

CN-L/ NSMP, copy-number low/ no specific molecular profile; IHC, immunohistochemistry; LVSI, lymphovascular space invasion; MMR, mismatch repair; MSI-H, microsatellite instability-high; RFS, recurrence free survival; WT, wild-type.

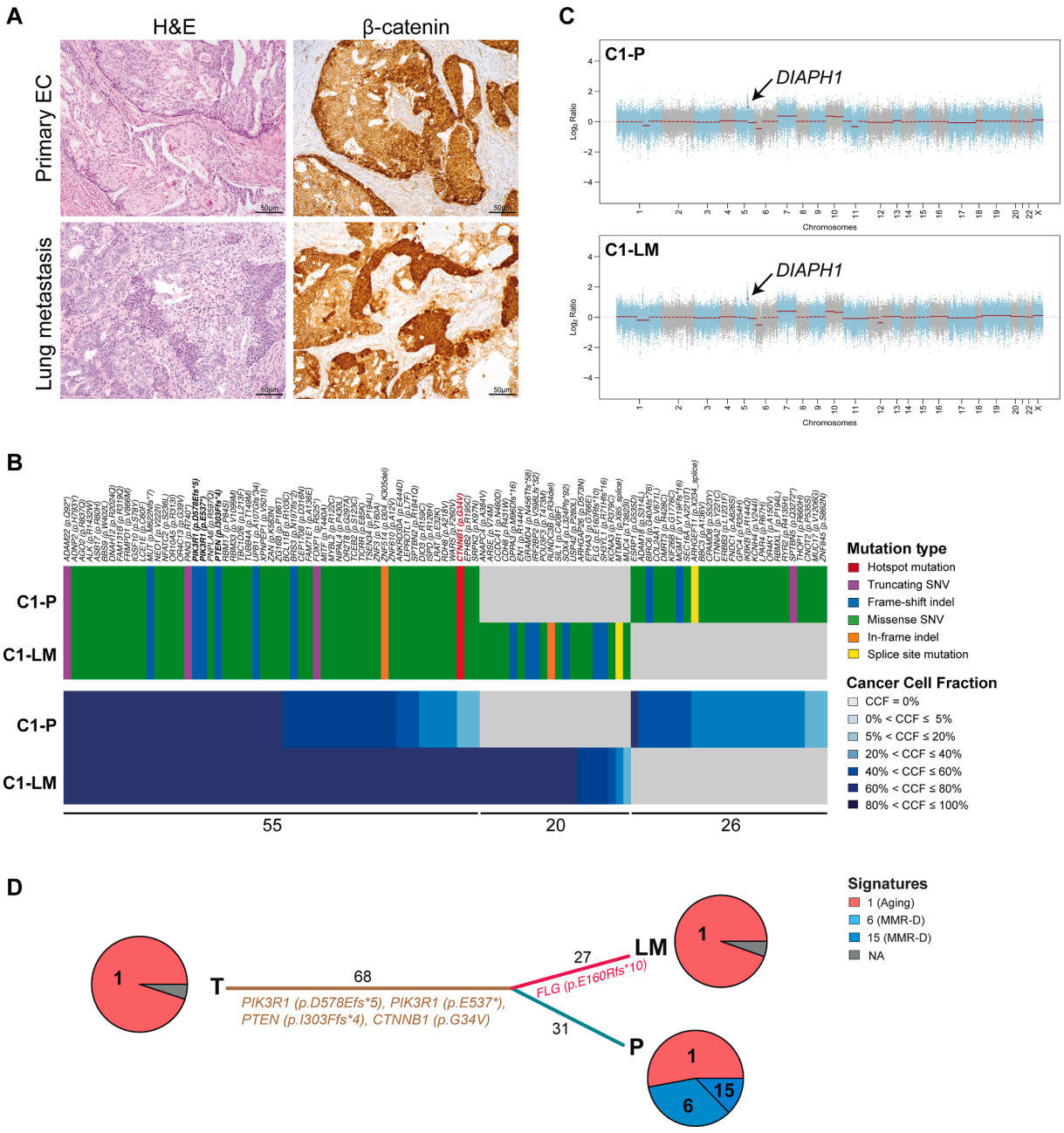

Fig. 1. Histopathologic and genomic analysis of the primary tumor and lung metastasis of Case 1. (A) Micrographs of representative hematoxylin and eosin–stained sections (left) and of the β-catenin immunohistochemical analysis (right) of the primary endometrial cancer and lung metastasis of Case 1. Scale bars, 50 μm. **(B)** Nonsynonymous somatic mutations identified by whole-exome sequencing in the primary tumor (C1-P) and lung metastasis (C1-LM). Mutation types and cancer cell fraction (CCF) of mutations identified are color coded according to the legend. The number of nonsynonymous mutations is shown at the bottom. **(C)** Copy-number alterations of the primary tumor (C1-P) and lung metastasis (C1-LM). Copy-number $\log_2$ ratios are shown on the y-axis according to the chromosomes on the x-axis. Arrow, amplification. **(D)** Mutational signature analysis performed on all mutations (synonymous and non-synonymous) and relationship among samples. Pie charts represent the mutational signatures identified in mutations shared between primary tumor and metastasis (trunk [T]), in mutations private to the primary tumor (C1-P) and the lung metastasis (C1-LM), color coded according to the legend. The length of the branches is proportional to the number of somatic mutations that are shared/unique to a given lesion and selected pathogenic somatic mutations and the number of all mutations is shown alongside the branches. MMR-D, DNA mismatch repair-deficiency; NA, not assigned; SNV, single nucleotide variant.

MSI-high molecular subtype (Table 1). A stepwise increase in the mutational burden was observed: the primary tumor (C2-P) harbored 670, the lung metastasis (C2-LM) 764; and the brain metastasis (C2-BrM) 820 nonsynonymous somatic mutations (Fig. 2**B**). Sixty-five clonal nonsynonymous somatic mutations were shared across the three lesions. In the primary tumor, 67 subclonal mutations including a hotspot mutation affecting *PIK3CA* (p.E545K) and a *PTEN* frameshift deletion (p.K267Rfs*9) became clonal in the lung and brain metastases (Fig. 2**B**). The primary tumor had a large number of somatic nonsynonymous mutations (n = 538) that were not shared with the lung or brain metastasis, including a private *CTNNB1* p.G34R hotspot mutation (Fig. 2**B**).

The lung and brain metastasis shared 707 nonsynonymous mutations which were not present in the primary tumors, including a clonal *PTEN* (p.V290*) loss-of-function mutation (Fig. 2**B**). One hundred subclonal mutations present in the lung metastasis became fully clonal in the brain

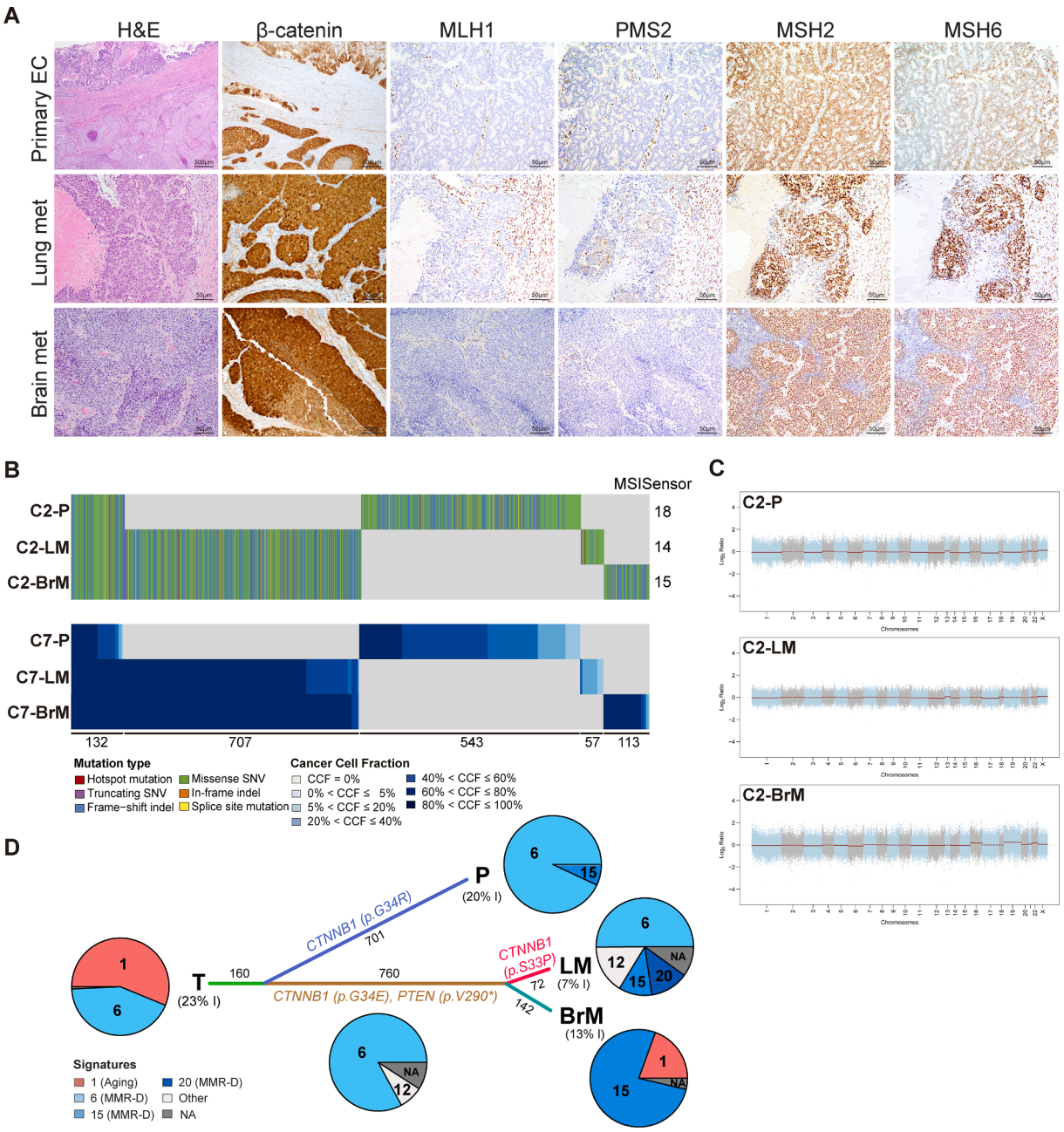

Fig. 2. Histopathologic and genomic analysis of the primary tumor, lung metastasis and brain metastasis of Case 2. (A) Micrographs of representative hematoxylin and eosin-stained sections and immunohistochemical analysis of β-catenin, MLH1, PMS2, MSH2 and MSH6 and β-catenin of the primary tumor, lung metastasis, and brain metastasis of Case 2. Scale bars, 500 μm top left two micrographs, remaining 50 μm. **(B)** Nonsynonymous somatic mutations identified by whole-exome sequencing in the primary tumor (C2-P), lung metastasis (C2-LM), and brain metastasis (C2-BrM). Mutation types and cancer cell fraction (CCF) of mutations identified are color coded according to the legend. The MSIsensor scores are shown on the right and the number of nonsynonymous mutations is shown on the bottom. **(C)** Copy-number alterations of the primary tumor (C2-P), lung metastasis (C2-LM) and brain metastasis (C2-BrM). Copy number $\log_2$ ratios are shown on the y-axis according to the chromosomes on the x-axis. **(D)** Mutational signature analysis of all mutations (synonymous and non-synonymous) and relationship among samples. Pie charts represent the mutational signatures identified in mutations shared between primary tumors and metastases (trunk [T]), in mutations shared between the metastases, and in mutations private to the primary tumor (C2-P), lung metastasis (C2-LM), and brain metastasis (C2-BrM), color coded according to the legend. The length of the branches is proportional to the number of somatic mutations that are shared/unique to a given lesion, the number of all mutations is shown alongside the branches, and selected pathogenic somatic mutations are shown alongside their corresponding branches. The percentage of small insertions and deletions (indels [I]) is included. MMR-D, DNA mismatch repair deficiency; NA, not assigned; SNV, single-nucleotide variant.

metastasis, including a hotspot *CTNNB1* p.G34E mutation (Fig. 2**B**). Of the 57 nonsynonymous mutations restricted to the lung metastasis, an additional subclonal *CTNNB1* (p.S33P) hotspot mutation was found, while in the brain metastasis, 113 non-synonymous mutations were found to be restricted to the brain metastases and absent in the primary tumor or lung metastasis (Fig. 2**B**). Immunohistochemical analysis revealed that while β-catenin exhibited membranous expression in the glandular component of the uterine primary, cytoplasmic and nuclear localization of β-catenin was restricted to the high-grade solid areas within the primary tumor and at metastatic sites (Fig. 2**A**). Finally, mutational signature analysis of the mutations shared between the three lesions revealed a dominant aging signature 1 as well as the MSI-related

signature 6 (Fig. 2**D**). In contrast, the mutations restricted to each of the components primarily harbored dominant MSI-related signatures, including 6, 15 and/or 20 (Fig. 2**D**).

4. Discussion

Here we demonstrate that both endometrioid ECs had branched evolution and that the primary EC and matched lung metastases had a common ancestor with independent evolution at each distant site. In addition, both cases displayed clonal shifts during the metastatic process to the lung with the accumulation of hotspot *CTNNB1* mutations.

In both cases, rather than additional copy number alterations, the ECs acquired additional mutations during the metastatic process (Nguyen et al., 2022). In Case 1, the lung metastasis had an increased mutational burden compared to the primary EC; and in Case 2, the brain metastasis had a higher mutational burden than the lung metastasis. Case 2 had *MLH1* hypermethylation and loss of MLH1 and PMS2 protein expression in the primary tumor and lung/ brain metastasis, and a shift from an aging to MMR mutational signatures was noted from primary to metastases, a phenomenon that has been previously described by our team (Dessources et al., 2020; Ashley et al., 2019). The acquisition of DNA repair defects and genomic instability may contribute to increasing mutational burden and development of metastasis.

ECs are classified into four molecular subtypes, including the *POLE* ultramutated, MSI-high, copy number-low/ NSMP and copy number-high/ p53abnormal (Cancer Genome Atlas Research Network et al., 2013). The cases studied here were of copy-number low/ NSMP (Case 1) and MSI-high (Case 2) molecular subtypes. About half (52 %) of microsatellite-stable copy-number low/ NSMP ECs harbor *CTNNB1* mutations (Cancer Genome Atlas Research Network et al., 2013). *CTNNB1* hotspot mutations have been reported to be associated with distant metastasis, and worse recurrence-free and overall survival in EC (Costigan et al., 2020; Weisman et al., 2022; Kurnit et al., 2017; Stelloo et al., 2016), however not all studies confirmed *CTNNB1* mutations to be an independent prognosticator of outcome in low-grade early-stage endometrioid EC (Safdar et al., 2022; Beshar et al., 2023). In fact, *CTNNB1* mutations have also been associated with low-risk pathologic features including grade 1–2 disease, lower rates of deep myometrial invasion and lympho-vascular space invasion (Kurnit et al., 2017).

In the current study, both endometrioid ECs harbored subclonal *CTNNB1* mutations that became clonal in the metastatic sites. Notably, the primary tumor of case 2 in this study had three *CTNNB1* hotspot mutations, however only the p.G34E mutation was present in the lung and brain metastases, providing evidence to suggest that certain hotspot mutations in *CTNNB1* may have a greater effect than others, even within the same hotspot codon. *CTNNB1* exon 3 hotspot mutation are generally associated with translocation of the protein product β-catenin from the membrane to the nucleus and activation of the Wnt/β-catenin signaling pathway. In EC, nuclear localization of β-catenin as assessed by immunohistochemistry has been shown to have high specificity in identifying *CTNNB1* mutant cases, but lower sensitivity, however, may be used as a proxy for *CTNNB1* mutation (Costigan et al., 2020; Kim et al., 2018; Travaglino et al., 2019). Further studies are warranted to define the subset of (early-stage) endometrioid ECs in which *CTNNB1* mutations and potentially β-catenin expression are associated with increased risk of recurrence/ metastasis to ultimately identify those patients who benefit from more aggressive surveillance and treatment. Also, Wnt inhibitors are currently being tested in clinical trials, which may play a role in cancers with high Wnt/β-catenin signaling activation (Jung and Park, 2020).

The results presented here, in combination with previously published work by our team and others (Dessources et al., 2020; Ashley et al., 2019; Nguyen et al., 2022), demonstrate the acquisition of additional mutations rather than copy number alterations during the distant metastatic process of EC, and support the notion of performing immunohistochemical and/or genomic analyses not only in the primary tumor but repeating it in metastatic sites of EC, as these may have acquired alterations or signatures during the metastatic process. Small, in-depth studies like the one presented here provide a deeper understanding of the genomics of EC, its progression, and development of distant metastasis. Based on these findings, further studies are warranted to identify the group of endometrioid ECs previously classified as low-risk (copy-number low/ NSMP) disease for which the presence of *CTNNB1* mutations can provide a further subclassification.

Funding

Research reported in this publication was supported in part by a Cancer Center Support Grant of the NIH/NCI (Grant No. P30CA008748). B. Weigelt is funded in part by Breast Cancer Research Foundation and Cycle for Survival, and NIH/NCI P50 CA247749 01 grants. F. Pareja is funded in part by the Starr Cancer Consortium and by the NIH/NCI P50 CA247749 01 grant.

Consent statement

IRB approval and written informed consent were obtained from both patients.

CRediT authorship contribution statement

Sushmita Gordhandas: Writing – review & editing, Writing – original draft, Investigation, Formal analysis, Data curation. **Arnaud Da Cruz Paula:** Writing – review & editing, Writing – original draft, Investigation, Formal analysis, Data curation. **Elizabeth C. Kertowidjojo:** Writing – review & editing, Writing – original draft, Investigation, Formal analysis, Data curation. **Fresia Pareja:** Writing – review & editing, Writing – original draft, Data curation. **Kimberly Dessources:** Writing – review & editing, Writing – original draft, Data curation. **Edaise M. da Silva:** Writing – review & editing, Writing – original draft, Data curation. **Fatemeh Derakhshan:** Writing – review & editing, Writing – original draft, Data curation. **Jennifer J. Mueller:** Writing – review & editing, Writing – original draft, Data curation. **Nadeem R. Abu-Rustum:** Writing – review & editing, Writing – original draft, Funding acquisition, Formal analysis. **M. Herman Chui:** Writing – review & editing, Writing – original draft, Formal analysis, Data curation. **Britta Weigelt:** Writing – review & editing, Writing – original draft, Supervision, Methodology, Investigation, Formal analysis, Conceptualization.

Declaration of competing interest

The authors declare the following financial interests/personal relationships which may be considered as potential competing interests: [B. Weigelt reports research funding from Repare Therapeutics and employment of an immediate family member at AstraZeneca, outside the submitted work. F. Pareja is a member of the scientific advisory board of MultiplexDx, and a member of the diagnostic advisory board and speaker for AstraZeneca. N.R. Abu-Rustum reports research funding from GRAIL paid to Memorial Sloan Kettering Cancer Center.].

References

Alexandrov, L.B., Nik-Zainal, S., Wedge, D.C., Aparicio, S.A., Behjati, S., Biankin, A.V., et al., 2013. Signatures of mutational processes in human cancer. Nature 500, 415–421.

Ashley, C.W., Da Cruz, P.A., Kumar, R., Mandelker, D., Pei, X., Riaz, N., et al., 2019. Analysis of mutational signatures in primary and metastatic endometrial cancer reveals distinct patterns of DNA repair defects and shifts during tumor progression. Gynecol. Oncol. 152, 11–19.

Beshar, I., Moon, A.S., Darji, H., Liu, C., Jennings, M.T., Dorigo, O., et al., 2023. Aberrant nuclear beta-catenin distribution does not prognosticate recurrences of endometrioid endometrial cancers - a retrospective single-institutional study. Gynecol. Oncol. 179, 85–90.

Cancer Genome Atlas Research Network, Kandoth C, Schultz N, Cherniack AD, Akbani R, Liu Y, et al. Integrated genomic characterization of endometrial carcinoma. Nature. 2013;497:67-73.

Costigan, D.C., Dong, F., Nucci, M.R., Howitt, B.E., 2020. Clinicopathologic and immunohistochemical Correlates of CTNNB1 mutated endometrial endometrioid Carcinoma. Int. J. Gynecol. Pathol. 39, 119–127.
Dessources, K., Da Cruz, P.A., Pareja, F., Stylianou, A., Cybulska, P., Farmanbar, A., et al., 2020. Acquisition of APOBEC mutagenesis and microsatellite instability signatures in the development of brain metastases in low-grade, Early-stage endometrioid endometrial Carcinoma. JCO Precis. Oncol. 4.
Gibson, W.J., Hoivik, E.A., Halle, M.K., Taylor-Weiner, A., Cherniack, A.D., Berg, A., et al., 2016. The genomic landscape and evolution of endometrial carcinoma progression and abdominopelvic metastasis. Nat. Genet. 48, 848–855.
Jung, Y.S., Park, J.I., 2020. Wnt signaling in cancer: therapeutic targeting of wnt signaling beyond beta-catenin and the destruction complex. Exp. Mol. Med. 52, 183–191.
Kim, G., Kurnit, K.C., Djordjevic, B., Singh, C., Munsell, M.F., Wang, W.L., et al., 2018. Nuclear beta-catenin localization and mutation of the CTNNB1 gene: a context-dependent association. Mod. Pathol. 31, 1553–1559.
Kurnit, K.C., Kim, G.N., Fellman, B.M., Urbauer, D.L., Mills, G.B., Zhang, W., Broaddus, R.R., 2017. CTNNB1 (beta-catenin) mutation identifies low grade, early stage endometrial cancer patients at increased risk of recurrence. Mod. Pathol. 30, 1032–1041.
Li, J., Sun, L., Zhang, Y., Cai, S., 2019. Patterns of distant metastases in patients with endometrial carcinoma: a SEER population-based analysis. J. Clin. Oncol. 37, e17109 -e.
Lu, K.H., Broaddus, R.R., 2020. Endometrial cancer. N. Engl. J. Med. 383, 2053–2064.
Mao, W., Wei, S., Yang, H., Yu, Q., Xu, M., Guo, J., Gao, L., 2020. Clinicopathological study of organ metastasis in endometrial cancer. Future Oncol. 16, 525–540.
Nguyen, B., Fong, C., Luthra, A., Smith, S.A., DiNatale, R.G., Nandakumar, S., et al., 2022. Genomic characterization of metastatic patterns from prospective clinical sequencing of 25,000 patients. Cell 185 (563–75), e11.
Safdar, N.S., Stasenko, M., Selenica, P., Martin, A.S., da Silva, E.M., Sebastiao, A.P.M., et al., 2022. Genomic determinants of Early recurrences in low-stage, low-grade endometrioid endometrial Carcinoma. J. Natl Cancer Inst. 114, 1545–1548.
Siegel, R.L., Giaquinto, A.N., Jemal, A., 2024. Cancer statistics, 2024. CA Cancer J. Clin. 74, 12–49.
Sohaib, S.A., Houghton, S.L., Meroni, R., Rockall, A.G., Blake, P., Reznek, R.H., 2007. Recurrent endometrial cancer: patterns of recurrent disease and assessment of prognosis. Clin. Radiol. 62, 28–34 discussion 5–6.
Stelloo, E., Nout, R.A., Osse, E.M., Jurgenliemk-Schulz, I.J., Jobsen, J.J., Lutgens, L.C., et al., 2016. Improved risk assessment by integrating Molecular and clinicopathological factors in Early-stage endometrial cancer-combined analysis of the PORTEC cohorts. Clin. Cancer Res. 22, 4215–4224.
Travaglino, A., Raffone, A., Saccone, G., De Luca, C., Mollo, A., Mascolo, M., et al., 2019. Immunohistochemical Nuclear expression of beta-catenin as a surrogate of CTNNB1 exon 3 mutation in endometrial cancer. Am. J. Clin. Pathol. 151, 529–538.
Weisman, P., Park, K.J., Xu, J., 2022. FIGO grade 3 endometrioid Adenocarcinomas with diffusely aberrant beta-catenin expression: an aggressive subset resembling cutaneous pilomatrix Carcinomas. Int. J. Gynecol. Pathol. 41, 126–131.